THE JOURNAL OF PHYSICAL CHEMISTRY C

Article

pubs.acs.org/JPCC

Insight into the Preference Mechanism of CH_x (x = 1−3) and C−C Chain Formation Involved in C_2 Oxygenate Formation from Syngas on the Cu(110) Surface

Riguang Zhang, Xuancheng Sun, and Baojun Wang*

Key Laboratory of Coal Science and Technology of Ministry of Education and Shanxi Province, Taiyuan University of Technology, Taiyuan 030024, Shanxi, People's Republic of China

ABSTRACT: The possible formation pathways of CH_x (x = 1−3) and C−C chain involved in C_2 oxygenate formation from syngas on an open Cu(110) surface have been systematically investigated to identify the preference mechanism of CH_x (x = 1−3) and C−C chain formation. Here, we present the main results obtained from periodic density functional calculations. Our results show that all CH_x (x = 1−3) species formation starts with CHO hydrogenation; among them, CH_x (x = 2, 3) are the most favored monomers, however, CH_3OH is the main product from syngas on the Cu(110) surface, and the formation of CH_x (x = 1−3) cannot compete with CH_3OH formation. Further, on the basis of the favored monomer CH_x (x = 2, 3), we probe into the C−C chain formation of C_2 oxygenates by CO or CHO insertion into CH_x (x = 2, 3), as well as the hydrogenation, dissociation, and coupling of CH_x (x = 2, 3), suggesting that CO insertion into CH_2 to form C_2 oxygenates is the dominant reaction for CH_2 on the Cu(110) surface with an activation barrier of 44.5 kJ·mol^{-1}; however, for CH_3, CH_3 hydrogenation to CH_4 is the dominant reaction on the Cu(110) surface with an activation barrier of 67.5 kJ·mol^{-1}. As a result, to achieve high productivity and selectivity for C_2 oxygenates from syngas, Cu has to get help from the promoters, which should be able to boost CH_2 formation and/or suppress CH_3OH and CH_3 formation. The present study provides the basis to understand and develop novel Cu-based catalysts for C_2 oxygenate formation from syngas.

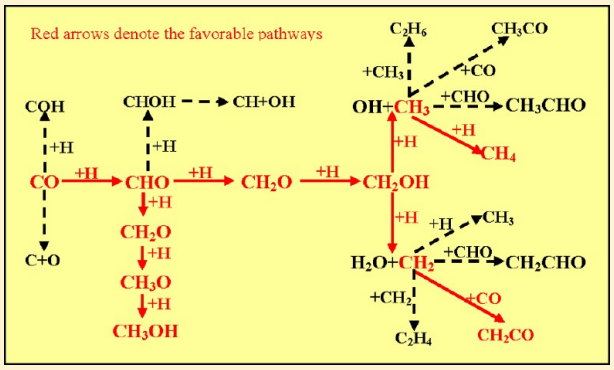

1. INTRODUCTION

Formation of C_2 oxygenates (typically referred to as ethanol, etc.) from syngas is an important industrial process for the production of clean liquid energy fuels and valuable chemical feedstocks.[1−6] Nowadays, one of the major obstacles for the application of C_2 oxygenates is the slow kinetics and low selectivity in C_2 oxygenate synthesis.[7] As a result, developing catalysts for synthesizing C_2 oxygenates efficiently and selectively has been one of the major challenges in catalysis. Up to now, Rh-based catalysts have shown promise, exhibiting high selectivity to C_2 oxygenate formation from syngas,[4−8] in which two key issues for the general mechanism of C_2 oxygenate formation are believed. One is the formation of surface hydrocarbon CH_x (x = 1−3) by the direct CO dissociation or hydrogen-assisted CO dissociation, and the other is the C−C chain formation.[4,5,9−14] However, the prohibitive cost and limited supply of Rh-based catalysts have restricted their ability to be used as industrial catalysts.[3,5] Therefore, much less expensive Cu-based catalysts have been an attractive option; nowadays, Cu-based catalysts have been widely used and produced promising results for C_2 oxygenate formation from syngas in the temperature range 280−310 °C at pressures of about 40−100 bar.[3,15−19] Recently, the progress about syngas to C_2 oxygenates on Cu-based catalysts has been reported in the review by Gupta et al.,[3] which suggests that there is the similarity for C_2 oxygenate formation from syngas between Cu-based and Rh-based catalysts, both involving two key steps: surface hydrocarbon CH_x (x = 1−3) and C−C chain formation.

For CH_x (x = 1−3) formation, two possibilities may exist. One is CO hydrogenation to form CH_xO species, followed by its dissociation (hydrogen-assisted CO dissociation mechanism); the other is the direct CO dissociation, followed by hydrogenation (carbide mechanism). For example, Choi and Liu[7] have found that CO hydrogenation to form formyl species (COH or CHO) is more plausible than the direct CO dissociation on the Rh(111) surface. Meanwhile, previous studies have also found that CH_3 is the most favorable monomer among all CH_x (x = 1−3) species on Co(0001)[20] and Rh(111)[7] surfaces. However, the studies by Kapur et al.[10] show that CH_2 is the most favored monomer among all CH_x (x = 1−3) species on Rh(111) and Rh(211) surfaces. On the other hand, for the C−C chain formation, one is that CO insertion into CH_x (x = 1−3) monomer leading to CH_xCO, and the other is that CHO insertion into CH_x (x = 1−3) monomer to form CH_xCHO; for example, Choi and Liu[7] have

Received: November 28, 2012
Revised: February 27, 2013
Published: March 18, 2013

   dx.doi.org/10.1021/jp311701r | J. Phys. Chem. C 2013, 117, 6594−6606

found the C−C chain formation by CO insertion into CH_3 on the Rh(111) surface. Meanwhile, the studies by Kapur et al.[10] have shown that CO insertion into CH_2 is deduced to be the precursor for C_2 oxygenate formation on Rh(111) and Rh(211) surfaces. Interestingly, Zhao et al.[14] have shown that CHO insertion is superior and/or competitive to CO insertion for C−C chain formation on Rh(111) and Co(0001) surfaces.

Up to now, although a large number of experimental studies on Cu-based catalysts as mentioned above have been performed to explore the C_2 oxygenate formation from syngas,[3,15−19] few studies have been carried out to fully understand the mechanism and kinetics about the above-mentioned two key issues, surface hydrocarbon CH_x (x = 1−3) and C−C chain formation involved in the C_2 oxygenate formation from syngas on Cu-based catalysts at the fundamental level due to the complexity of the reactions. As a result, on Cu-based catalysts, the mechanism and kinetics of CH_x (x = 1−3) and C−C chain formation involved in C_2 oxygenate formation from syngas still remain unclear: Are surface hydrocarbon species, CH_x (x = 1−3), formed by the hydrogen-assisted CO dissociation mechanism or the carbide mechanism? Besides, among all CH_x (x = 1−3) species, which is the most favored monomer? On the other hand, is the C−C chain formed by CO or CHO insertion into CH_x (x = 1−3) monomer? Therefore, it is very necessary and significant to probe into the preference mechanism of CH_x (x = 1−3) and C−C chain formation involved in C_2 oxygenate formation from syngas on Cu catalyst. Nowadays, state-of-the-art theoretical investigations have been used as a powerful tool to elucidate the mechanism and kinetics of several typical reactions.[21−28] By means of theoretical calculation, a detailed investigation of CH_x (x = 1−3) and C−C chain formation involved in C_2 oxygenate formation from syngas on Cu catalyst at the molecular level will not only help us better understand the underlying preference mechanisms but also serves as a basis for the selective modification and development of novel Cu-based catalysts to improve the catalytic performance toward the desired C_2 oxygenates. For example, Choi and Liu[7] have investigated the mechanism of C_2 oxygenate formation on the Rh(111) surface on the basis of DFT calculations. They found that CH_3 is the most favorable monomer among all the CH_x species, and the selectivity to C_2 oxygenates on Rh(111) is controlled by methane formation by CH_3 hydrogenation and C−C bond formation by CO insertion into CH_3, and suggested that the metal Fe promoters, which can suppress methane formation and/or boost C−C bond formation, are indispensable to achieve high productivity and selectivity for ethanol.

In this paper, in order to identify the preference formation mechanism of CH_x (x = 1−3) and C−C chain, density functional theory together with periodic slab model calculations have been employed to investigate the possible pathways of CH_x (x = 1−3) and C−C chain formation involved in C_2 oxygenate formation from syngas on Cu catalyst at the molecular level. An open Cu(110) surface is chosen to model Cu catalyst, and the mechanism and kinetics of CH_x (x = 1−3) and C−C chain formation on the Cu(110) surface are systematically investigated, in which a large number of unique reaction pathways involving subtly different reaction intermediates and transition states are explicitly obtained. Further, the results of this effort are expected to qualify the activation barriers and reaction energies of elementary steps involved in the pathways of CH_x (x = 1−3) and C−C chain formation, and obtain the preference formation mechanism of CH_x (x = 1−3) and C−C chain. Finally, our results are expected to serve as a basis for the selective modification of Cu catalyst to improve catalytic performance toward C_2 oxygenate formation from syngas. In addition, our calculation may be a worthwhile theoretical example for the CH_x (x = 1−3) and C−C chain formation involved in C_2 oxygenate formation from syngas on other metal or alloy surfaces.

2. COMPUTATIONAL DETAILS

2.1. Surface Model. Previous experimental studies[29−31] have shown that methanol decomposition into methoxy mainly occurs on the Cu(110) surface; the other two low-index Cu surfaces, Cu(111) and Cu(100), are inactive to methanol decomposition; moreover, the studies by Nakamura et al.[32] suggested that the dissociation of H_2O on Cu(110) seems to be more favorable than that on Cu(111), which is also supported by other relevant studies.[33−35] These studies indicate that the Cu(110) surface may be more active due to its more open surface and more coordinative unsaturated sites. Thus, in this study, an open Cu(110) surface is chosen to model Cu catalyst, and to investigate the mechanism and kinetics of the CH_x (x = 1−3) and C−C chain formation on Cu catalyst.

In the surface calculation, the Cu(110) surface is cleaved from the experimental fcc crystal structure with a lattice parameter of 3.62 Å,[36] and is modeled using a three-atomic-layer $p(3 \times 3)$ super cell with nine atoms at each layer; this corresponds to a 1/9 monolayer (ML) coverage. Meanwhile, a 15 Å vacuum slab is employed to separate the periodically repeated slabs. The bottom one layer is constrained at the bulk position in order to mimic the presence of a larger number of layers in real metal particles, whereas the upper two layers together with the adsorbed species involved in CH_x (x = 1−3) and C−C chain formation are allowed to relax. According to Cu(110)−[3 × 3] surface morphology, as shown in Figure 1, there are four different adsorption sites: top (T), long bridge (LB), short bridge (SB), and hollow (H).

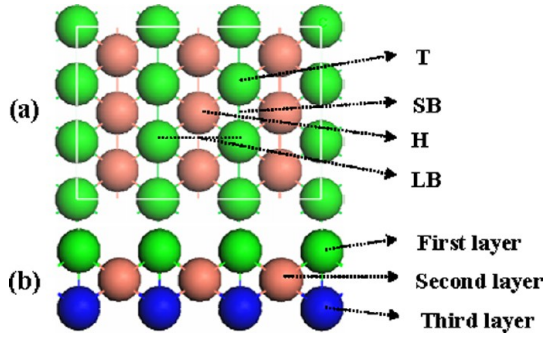

Figure 1. The surface configuration and adsorption sites of the Cu(110) surface: (a) top view; (b) side view.

2.2. Calculation Methods. Plane-wave DFT calculations with the projector-augmented wave (PAW) method[37] are carried out as implemented in the Vienna ab initio simulation package (VASP).[38−40] The generalized gradient approximation with the Perdew−Wang exchange-correlation functional (GGA-PW91) is used.[41] The kinetic energy cutoff for a plane wave basis set is 400 eV. The Brillouin zone is sampled using a 3 × 3 × 1 Monkhorst−Pack k-point grid (11 k-points)[42] with Methfessel−Paxton smearing of 0.1 eV.[43] The relaxation of the electronic degrees of freedom is assumed to be converged if the total energy change and the band structure energy change

dx.doi.org/10.1021/jp311701r | J. Phys. Chem. C 2013, 117, 6594−6606

between two steps are both smaller than 10^{-5} eV. A force difference between two steps less than 0.03 eV/Å is used as the criterion for convergence of relaxation.

Reaction paths have been studied using the climbing-image nudged elastic band method (CI-NEB).[44,45] Transition states have been optimized using the dimer method.[46,47] The transition state structure is deemed converged when the forces acting on the atoms are all <0.05 eV/Å for the various degrees of freedom set in the calculation. The molecules in the gas phase (needed to obtain adsorption energies) are calculated using a 10 × 10 × 10 Å^3 cubic unit cell.

2.3. Evaluation of Calculation Method and Model. To investigate the reliability of the selected method and model, we first calculate the geometrical parameters of free CO molecule in the gas phase. The bond length and the stretching frequency of CO are r_{C-O} = 1.142 Å and ν_{C-O} = 2125 cm^{-1}, respectively, which are in agreement with the experimental values of 1.128 Å[48] and ν_{C-O} = 2138[49] and 2143 cm^{-1},[50−52] respectively. Meanwhile, our calculated result is close to other DFT calculated values obtained by Sun et al. (2121 cm^{-1}),[49] Weilach et al. (2120 cm^{-1}),[51] and Loffreda et al. (2106 cm^{-1}).[52]

Then, to confirm the sufficiency of the chosen model (three-layer and super cell of $p(3 \times 3)$ Cu), we further compare the adsorption of CO at the SB site with those obtained on four-layer and five-layer $p(3 \times 3)$ models (the top two layers with adsorbates are relaxed, and the other bottom layers are fixed to their buck positions). The adsorption energies of CO are 109.5 and 105.2 (111.1) kJ·mol^{-1} with CO bond lengths of 1.170 and 1.170 (1.171) Å, which are close to the values obtained by using a three-layer $p(3 \times 3)$ model (see the values in parentheses, which will be obtained in the section below).

Further, to consider the effect of surface coverage on calculated results, we test the adsorption of the largest system CH_2CHO mentioned in our study at the most stable hollow site on a $p(2 \times 2)$, $p(2 \times 3)$, and $p(4 \times 4)$ three-layer model. The corresponding adsorption energies of CH_2CHO are 260.1, 270.9, and 273.3 kJ·mol^{-1}, respectively. We can obtain that the adsorption energies of CH_2CHO on the $p(2 \times 3)$ (270.9 kJ·mol^{-1}) and $p(4 \times 4)$ (273.3 kJ·mol^{-1}) models are close to the value 269.4 kJ·mol^{-1} obtained by using a $p(3 \times 3)$ model. Therefore, considering the efficiency of calculation, we think that a three-layer $p(3 \times 3)$ model is suitable and enough for our calculated systems.

Finally, the three-layer (110) surface model has been widely used in the previous calculations of reactions on the metal surface; for example, Flemmig et al.[53] used a three-layer slab Mo(110) surface to investigate the mechanism for the transformation of adsorbed cyclopropylmethyloxide; Classen et al.[54] investigated the interaction of trimesic acid with a three-layer slab Cu(110) surface; Wang et al.[55] studied the adsorption of CH_3, CH_3O, and HCOO on metal Ni using a three-layer slab Ni(110) surface model; Szukiewicz et al.[56] employed a three-layer slab Mo(110) surface to investigate the Gd adsorbed layers on the Mo(110) surface; Liao et al.[57] used a three-layer slab Rh(110) surface to investigate the adsorption of NO.

Therefore, according to the above evaluations together with previous studies about a three-layer slab (110) model, we are confident in the ability of the chosen method and model to describe the mechanism and kinetics for CH_x (x = 1−3) and C−C chain formation involved in C_2 oxygenate formation from syngas on a three-layer slab $p(3 \times 3)$ Cu(110) model.

3. RESULTS AND DISCUSSION

In this section, we first investigate the mechanism of CH_x (x = 1−3) formation according to the proposed reaction network of CH_x (x = 1−3) formation by CO hydrogenation, in which the adsorption energies and structures of the important intermediates involved in CH_x (x = 1−3) formation on the Cu(110) surface are obtained, and these results are compared with previously reported theoretical and experimental observations; then, we describe the transition states associated with every elementary step in the reaction network of CH_x (x = 1−3) formation to obtain the most favored CH_x monomer. On the other hand, on the basis of the most favored CH_x monomer, the possible pathways of C−C chain formation are further investigated to probe into the preference formation mechanism. Finally, we generally discuss the potential energy surface for the formation of CH_x (x = 1−3) and C−C chain of C_2 oxygenates, as well as other possible reactions involved in C_2 oxygenate formation from syngas, such as CH_3OH formation, CH_x hydrogenation and dissociation, and the coupling of CH_x to form C−C chain.

3.1. CH_x (x = 1−3) Formation by CO Hydrogenation.

3.1.1. Reaction Network of CH_x (x = 1−3) Formation. Previous studies have investigated the formation of CH_3OH from syngas through CHO, COH, CH_2O, CHOH, CH_3O, and CH_2OH intermediates.[36,58,59] Meanwhile, Iglesia et al.[60] have studied the CO direct dissociation and H-assisted CO dissociation through CHO and CHOH intermediates on both Fe and Co catalysts, suggesting that H-assisted CO dissociation is more favorable than CO direct dissociation; Zhang et al.[61] have also researched the CO direct dissociation and H-assisted CO dissociation through COH, CHO, CHOH, and CH_2O intermediates on the Ni(111) surface, suggesting that CO prefers to hydrogenate rather than direct dissociation; Li et al.[62] have investigated the CO direct dissociation and H-assisted CO dissociation through CHO intermediate on the Fe(111) surface, suggesting that CO prefers to form CHO intermediate rather than CO direct dissociation, then, the dissociation of CHO into CH+O is more favorable both thermodynamically and kinetically than CHO hydrogenation; Kapur et al.[10] investigated the CO direct dissociation and H-assisted CO dissociation through COH, CHO, CHOH, CH_2O, CH_2OH, and CH_3O intermediates on Rh catalyst, suggesting that H-assisted CO dissociation to form CH_x is more favorable than CO direct dissociation.

Therefore, on the basis of the above literature about CO hydrogenation and dissociation on different metal catalysts, in this study, the reaction network of CH_x (x = 1−3) formation from CO hydrogenation and dissociation on the Cu(110) surface has been proposed, as displayed in Figure 2, which covers all possible pathways of CH_x (x = 1−3) formation. The adsorbed CO can dissociate via a series of sequential steps to form CH_x (x = 1−3), in which two possibilities for CH_x (x = 1−3) formation exist; one is the CO hydrogenation to form C_1 oxygenated entities, followed by its dissociation without or with hydrogen-assistance to form CH_x (x = 1−3); the other is the CO direct dissociation to form C and O atoms, followed by C hydrogenation to form CH_x (x = 1−3). By investigating the mechanism and kinetics of the proposed reaction network of CH_x (x = 1−3) formation, an optimal path for CH_x (x = 1−3) formation will be identified.

3.1.2. Adsorptions of Reactants and Possible Intermediates. The adsorption energy is always regarded as a measure of

dx.doi.org/10.1021/jp311701r | J. Phys. Chem. C 2013, 117, 6594−6606

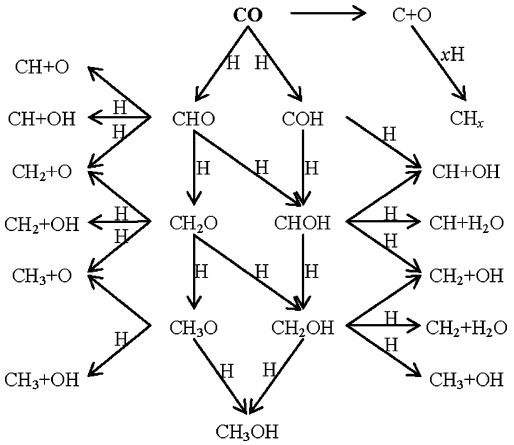

Figure 2. Reaction network scheme of CH_x (x = 1−3) formation by CO hydrogenation and dissociation.

the strength of adsorbate−Cu(110) substrate adsorption. The adsorption energies, E_{ads}, are defined as follows:

$$E_{ads} = E_{Cu(110)} + E_{adsorbate} - E_{adsorbate/Cu(110)}$$

where $E_{Cu(110)}$ is the energy of a clean Cu(110) slab, $E_{adsorbate}$ is the energy of free adsorbate, and $E_{adsorbate/Cu(110)}$ is the total energy of the adsorbate/Cu(110) system in the equilibrium state. With this definition, more positive values reflect the strong interaction of adsorbed species with the Cu(110) surface.

Adsorptions of the reactants and all possible intermediates involved in CH_x (x = 1−3) formation on the Cu(110) surface have been investigated. Figure 3 presents the most stable adsorption configurations of these species, and the corresponding key geometric parameters are listed in Table 1.

C, O, and H. C and O prefer to adsorb at the H site on the Cu(110) surface, as shown in Figure 3. The distance between C and Cu atoms is 1.99 Å, and the corresponding adsorption energy is 689.3 kJ·mol^{-1}. The distance between O and Cu atoms is 2.10 Å, and the corresponding adsorption energy is 656.9 kJ·mol^{-1}. For H atom, the stable adsorption site is the pseudo-fcc(111) site, and the corresponding adsorption energy is 357.3 kJ·mol^{-1}; the bond lengths of H−Cu are 1.69, 1.69, and 1.86 Å, respectively.

CO, OH, and CH_3. CO, OH, and CH_3 prefer to adsorb at the SB site on the Cu(110) surface, as shown in Figure 3. We can see that both CO and CH_3 tend to coordinate to the surface through a C atom; OH tends to coordinate to the surface through an O atom. The adsorption energy of CO is 111.1 kJ·mol^{-1} with the Cu−C bond length of 1.97 Å. The Cu−O and O−H bond lengths for adsorbed OH are 1.95 and 0.98 Å, respectively, and the corresponding adsorption energy is 403.9 kJ·mol^{-1}. The adsorption energy of CH_3 is 246.5 kJ·mol^{-1} with two C−Cu bond lengths of 2.05 and 2.13 Å, respectively.

CH, CH_2, COH, and CH_2O. CH, CH_2, COH, and CH_2O all prefer to adsorb at the H site on the Cu(110) surface, as shown in Figure 3. The adsorption energy of CH is 603.3 kJ·mol^{-1} with a C−Cu distance of 2.07 Å. The adsorption energy of CH_2 is 414.2 kJ·mol^{-1} with four C−Cu bond lengths of 2.25, 2.26, 2.27, and 2.27 Å, respectively. COH tends to coordinate to the surfaces through a C atom with an adsorption energy of 340.3 kJ·mol^{-1}; CH_2O binds to the surface through both O atom anchoring at the SB site and C atom sitting at another SB site with an adsorption energy of 78.6 kJ·mol^{-1}.

CHO, CHOH, CH_2OH, and CH_3O. The most stable configuration for CHO adsorbed at the LB site through both C and O atoms has an adsorption energy of 219.9 kJ·mol^{-1}. CHOH prefers to bind at the SB site on Cu(110) through a C atom with the hydroxyl H atom pointing toward the surface, which is in agreement with previous DFF calculations.[63] CH_2OH prefers to bind at the SB site on Cu(110) through both C and O atoms. CH_3O binds at the SB site through an O atom. Our results agree with the experimental results,[64] in which the ultraviolet photoelectron spectroscopy (UPS) experiment shows that CH_3O adsorbs on the Cu(110) surface through an O atom with an off-normal orientation.

H_2O and CH_3OH. H_2O prefers to adsorb at the T site on the Cu(110) surface with an adsorption energy of 55.1 kJ·mol^{-1}. CH_3OH binds at the T site through an O atom with an adsorption energy of 63.5 kJ·mol^{-1}; more interestingly, previous experimental estimation for the adsorption energy of CH_3OH is 67.5 kJ·mol^{-1} from first-order temperature-programmed desorption (TPD);[65] our calculated results agree with the experimental results.

3.1.3. CO Hydrogenation and Dissociation. As shown in Figure 2, there are two possibilities for CO: one is CO direct dissociation to form C and O; the other is CO hydrogenation to form CHO or COH. The potential energy diagram for the above three reactions together with the structures of the initial states, transition states, and final states are illustrated in Figure 4.

For CO direct dissociation, the C−O bond activation of CO via a transition state TS1 can lead to a final state, C+O; in TS1, the CO molecule stays almost horizontally on the surface with an elongated C−O bond length of 1.98 Å. This elementary reaction is highly endothermic by 213.4 kJ·mol^{-1} with a significantly high activation barrier of 409.1 kJ·mol^{-1}, which means that direct CO dissociation on the Cu(110) surface is likely to be very difficult.

For CO hydrogenation, there are two possibilities: one is that with H attacking at the C atom of CO to produce CHO; the

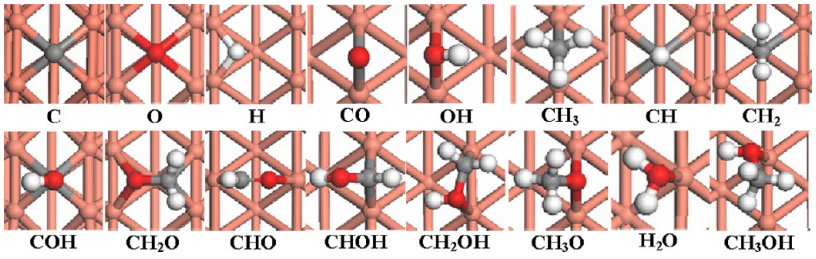

Figure 3. The most stable configurations of the reactants and all possible intermediates at their favorable sites involved in the formation of CH_x (x = 1−3) species on the Cu(110) surface. The C, O, H, and Cu atoms are shown in the gray, red, white, and orange balls, respectively.

dx.doi.org/10.1021/jp311701r | J. Phys. Chem. C 2013, 117, 6594−6606

Table 1. Adsorption Energies and Key Geometric Parameters for Various Relevant Species Involved in the Formation of CH_x (x = 1−3) on the Cu(110) Surface

species	E_{ads} (kJ·mol^{-1})	adsorption configuration	D_{Cu-X} (Å)	bonding details	
				bond	length (Å)
C	689.3	H: through C	1.99		
O	656.9	H: through O	2.10		
H	357.3	H: through H	1.69/1.86/1.69		
CO	111.1	SB: through C	1.97	C—O	1.17
OH	403.9	SB: through O	1.95	O—H	0.98
CH_3	246.5	SB: through C	2.05/2.13	C—H	1.12/1.10/1.10
CH	603.3	H: through C	2.07	C—H	1.11
CH_2	414.2	H: through C	2.25/2.26/2.27/2.27	C—H	1.11
COH	340.3	H: through C	2.08/2.08/2.08/2.09	C—O/O—H	1.38/0.98
CH_2O	78.6	H: C-SB, O-SB	2.20/2.01	C═O/C—H	1.39/1.11
CHO	219.9	LB: C-T, O-T	1.92/2.03	C—O/C—H	1.25/1.12
CHOH	255.7	SB: through C	1.99	C—H/C—O/O—H	1.10/1.35/1.00
CH_2OH	203.6	SB: C-T, O-T	1.98/2.14	C—H/C—O/O—H	1.10/1.46/0.99
CH_3O	311.7	SB: through O	1.95	C—O/C—H	1.43/1.10/1.10/1.11
H_2O	55.1	T: through O	2.20	O—H	0.98
CH_3OH	63.5	T: through O	2.14	C—H/C—O/O—H	1.10/1.45/0.98

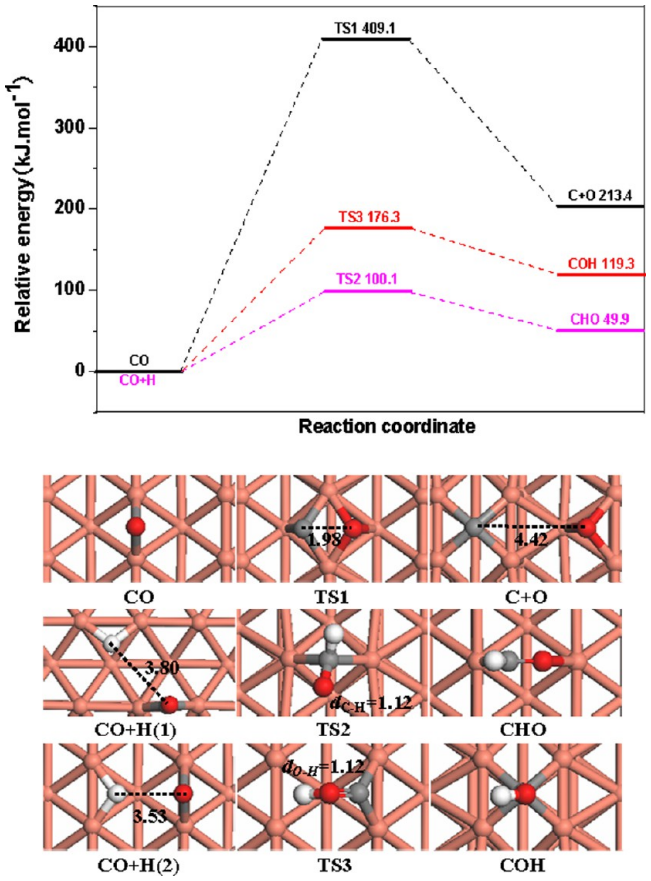

Figure 4. The potential energy profile for CO hydrogenation and dissociation together with the structures of the initial states, transition states (TS), and final states. Bond lengths are in Å. See Figure 3 for color coding.

other is that with H attacking at the O atom of CO to form COH. For CHO formation, starting from the initial state, CO +H(1), CO adsorbs at the SB site and H binds at the pseudo-fcc(111) site; both are the most stable configuration for CO and H species on the Cu(110) surface. The H adatom moves toward the C atom of adsorbed CO, forcing the vertically adsorbed CO to tilt from the surface normal in the transition state TS2, and the distance between C and H atoms in TS2 decreases to 1.12 Å from 3.80 Å in CO+H(1). The activation barrier for this elementary reaction is 100.1 kJ·mol^{-1}, and the reaction is found to be endothermic by 49.9 kJ·mol^{-1}. For COH formation, beginning with the initial state, CO+H(2), the H adatom moves toward the O atom of adsorbed CO via a transition state TS3 to form COH. In TS3, the distance between O and H atoms is shortened to 1.12 Å from 3.53 Å in CO+H(2); this elementary reaction is found to be endothermic by 119.3 kJ·mol^{-1} with a high activation barrier of 176.3 kJ·mol^{-1}.

On the basis of the above results, we can obtain that CHO formation is more favorable both kinetically and thermodynamically than COH formation and CO direct dissociation, indicating that CHO is the dominant product for CO hydrogenation on the Cu(110) surface.

3.1.4. CH Formation. As mentioned above, CHO is the dominant product for CO hydrogenation on the Cu(110) surface; as a result, in this study, we only consider CH_x (x = 1−3) formation starting from CHO and CHO hydrogenation.

As shown in Figure 2, there are four pathways for CH formation from CHO and CHO hydrogenation: Path 1-1 is the C−O bond scission of CHO to form CH and O; path 1-2 is the C−O bond scission of CHO with hydrogen assistance to form CH and OH; path 1-3 is CHO hydrogenation to form CHOH, followed by the C−O bond scission of CHOH to form CH and OH; path 1-4 is CHO hydrogenation to form CHOH, followed by the C−O bond scission of CHOH with hydrogen assistance to form CH and H_2O. The potential energy diagram for these reactions together with the structures of initial states, transition states, and final states are shown in Figure 5.

For path 1-1, starting from CHO, the C−O bond scission of CHO can form CH and O via a transition state TS1-1. In TS1-1, CH binds at the SB site through a C atom and O adsorbs at the LB site with a substantially elongated C−O bond of 2.40 Å. In the final state, CH+O, CH sits at the H site and O binds at the pseudo-fcc(111) site. This elementary reaction is endothermic by 44.7 kJ·mol^{-1} with a higher activation barrier of 231.6 kJ·mol^{-1}.

dx.doi.org/10.1021/jp311701r | J. Phys. Chem. C 2013, 117, 6594−6606

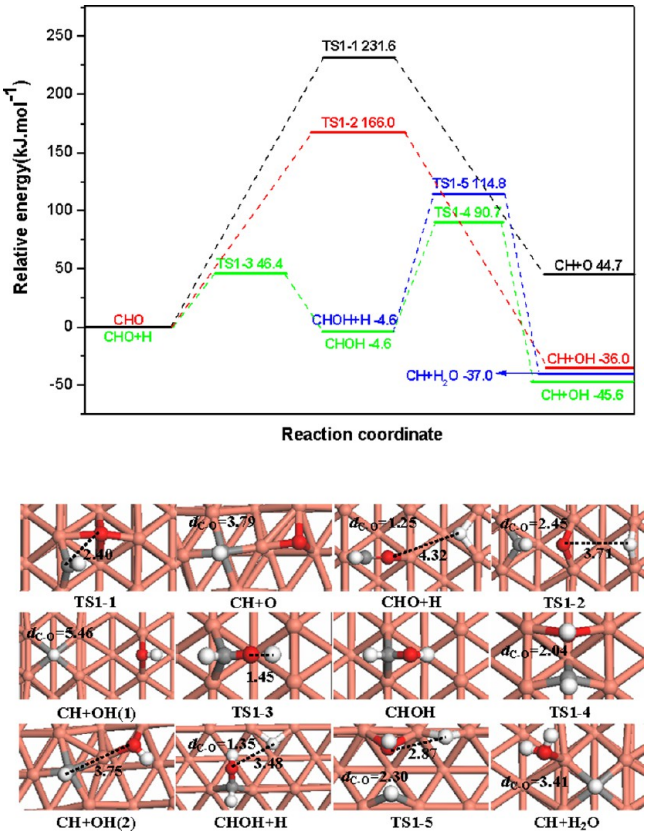

Figure 5. The potential energy profile for CH formation together with the structures of initial states, transition states, and final states. Bond lengths are in Å. See Figure 3 for color coding.

For path 1-2, the C−O bond scission of CHO with hydrogen assistance can form CH and OH via a transition state TS1-2. In TS1-2, a H adatom locates at the SB site, an O atom binds at another SB site with a substantially shortened distance between H adatom and O of 3.71 Å, and CH adsorbs at the pseudo-fcc(111) site through a C atom. In the final state, CH+OH(1), CH adsorbs at the H site and OH adsorbs at the SB site; both are the most stable configuration of CH and OH species on the Cu(110) surface, respectively. This elementary reaction is found to be exothermic by 36.0 kJ·mol^{-1} and has an activation barrier of 166.0 kJ·mol^{-1}.

For path 1-3, the H adatom first attacks the O atom of CHO to form CHOH via a transition state TS1-3. In TS1-3, the distances between the H adatom and O decrease to 1.45 Å from 4.32 Å in CHO+H. This elementary reaction has a small activation barrier of 46.4 kJ·mol^{-1}, and is found to be slightly exothermic by 4.6 kJ·mol^{-1}. Subsequently, the C−O bond scission of CHOH can lead to the formation of CH and OH via TS1-4. In TS1-4, CH binds at the LB site through a C atom; OH sits at the LB site through an O atom with an elongated C−O bond of 2.04 Å. In the final state, CH+OH(2), CH locates at the H site and OH binds at the SB site with a distance between C and O atoms of 3.75 Å. This elementary reaction needs to overcome an activation barrier of 95.3 kJ·mol^{-1}, and the reaction is exothermic by 41.0 kJ·mol^{-1}.

For path 1-4, as described in path 1-3, CHO first hydrogenates to form CHOH; then, the C−O bond scission of CHOH with hydrogen assistance can form CH+H$_2$O via a transition state TS1-5. In TS1-5, CH binds at the SB site through a C atom, OH locates at the pseudo-fcc(111) site through an O atom with an elongated C−O bond of 2.30 Å, and atomic H sits at the SB site. The activation barrier and reaction energy for this elementary reaction are found to be 119.4 and −32.4 kJ·mol^{-1}, respectively.

On the basis of the above results, starting from CHO and CHO+H, we can see from Figure 5 that the highest barriers for paths 1-1, 1-2, 1-3, and 1-4 are 231.6, 166.0, 90.7, and 114.8 kJ·mol^{-1} with the corresponding reaction energies of 44.7, −36.0, −45.6, and −37.0 kJ·mol^{-1}, respectively, suggesting that path 1-3 (CHO + H → CHOH → CH + OH) is more favorable both kinetically and thermodynamically than other pathways, which means that path 1-3 is mainly responsible for CH formation from CHO hydrogenation on the Cu(110) surface. The rate-controlled step for path 1-3 occurs at TS1-4 with a corresponding activation barrier of 95.3 kJ·mol^{-1}.

3.1.5. CH_2 Formation. As shown in Figure 2, there are eight possible pathways for CH_2 formation. The corresponding potential energy diagram for these reaction pathways together with the initial states, transition states, and final states are illustrated in Figure 6.

For path 2-1, the C−O bond scission of CHO with hydrogen assistance leads to the formations of CH_2 and O via a transition state TS2-1. In TS2-1, CH sits at the SB site through a C atom,

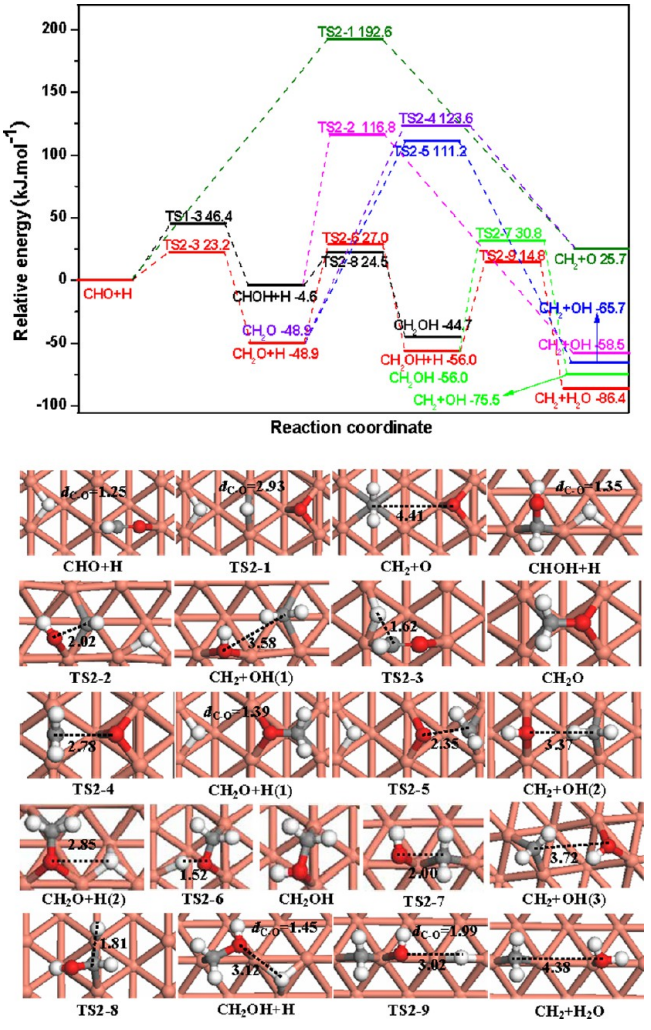

Figure 6. The potential energy profile for CH_2 formation together with the structures of initial states, transition states, and final states. Bond lengths are in Å. See Figure 3 for color coding.

dx.doi.org/10.1021/jp311701r | J. Phys. Chem. C 2013, 117, 6594−6606

atomic O binds at the pseudo-fcc(111) site with an elongated distance between C and O atoms of 2.93 Å, and atomic H locates at the pseudo-fcc(111) site. In the final state, CH_2+O, CH_2 adsorbed at the H site and O adsorbed at the pseudo-fcc(111) site with the distance between C and O atoms of 4.41 Å. This elementary reaction is endothermic by 25.7 kJ·mol^{-1}, and has a high activation barrier of 192.6 kJ·mol^{-1}.

For path 2-2, as described in path 1-3, CHO first hydrogenates to form CHOH; then, the C−O bond scission of CHOH with hydrogen assistance goes through a transition state TS2-2 to form CH_2 and OH. In TS2-2, the C−O bond is elongated to 2.02 Å from 1.35 Å in CHOH+H. In the final state, CH_2+OH(1), CH_2 locates at the H site through a C atom and OH locates at the SB site through an O atom with a distance between C and O atoms of 3.58 Å. The activation barrier for this elementary reaction is 121.4 kJ·mol^{-1}, and the reaction is found to be exothermic by 53.9 kJ·mol^{-1}.

For path 2-3, CHO first hydrogenates to form CH_2O via TS2-3. In TS2-3, CHO binds at the LB site through both C and O atoms; H binds at the SB site. This elementary reaction is exothermic by 48.9 kJ·mol^{-1}, and has a lower activation barrier of 23.2 kJ·mol^{-1}. Subsequently, the C−O bond cleavage of CH_2O can form CH_2 and O via TS2-4. In TS2-4, CH_2 adsorbs at the SB site through a C atom and O locates at the pseudo-fcc(111) site with an elongated distance between C and O atoms of 2.78 Å. The activation barrier for this elementary reaction is 172.5 kJ·mol^{-1}, and the reaction is found to be endothermic by 74.6 kJ·mol^{-1}.

For path 2-4, as described in path 2-3, CHO first hydrogenates to form CH_2O; then, the C−O bond scission of CH_2O with hydrogen assistance can form CH_2 and OH via TS2-5. In TS2-5, CH_2 locates at the pseudo-fcc(111) site through a C atom, O adsorbs at the pseudo-fcc(111) site, and the H adatom binds at the pseudo-fcc(111) site. In the final state, CH_2+OH(2), CH_2 locates at the SB site through a C atom and OH binds at the SB site through an O atom. This elementary reaction is exothermic by 16.8 kJ·mol^{-1}, and has a high activation barrier of 160.1 kJ·mol^{-1}.

For path 2-5, as described in path 2-3, CHO first hydrogenates to form CH_2O; then, the hydrogenation of CH_2O can form CH_2OH via TS2-6. After that, the C−O bond scission of CH_2OH leads to CH_2 and OH via TS2-7. The elementary reaction via TS2-6 has a lower activation barrier of 75.9 kJ·mol^{-1}, and the reaction is found to be slightly exothermic by 7.1 kJ·mol^{-1}. The activation barrier for the elementary reaction via TS2-7 is 86.8 kJ·mol^{-1}, and the reaction is exothermic by 19.5 kJ·mol^{-1}.

For path 2-6, CHO first hydrogenates to form CHOH, followed by CHOH hydrogenation to form CH_2OH. After that, the C−O bond scission of CH_2OH occurs to form CH_2 and OH. CHO hydrogenation to form CHOH and the dissociation of CH_2OH to form CH_2 and OH have been described in paths 1-3 and 2-5; thus, we only describe CHOH hydrogenation to form CH_2OH via TS2-8; this elementary reaction is exothermic by 40.1 kJ·mol^{-1} and needs to overcome a small activation barrier of 29.1 kJ·mol^{-1}.

For paths 2-7 and 2-8, path 2-7 is that via path 2-5 (CH_2O intermediate) to form CH_2OH; after that, the C−O bond scission of CH_2OH with hydrogen assistance to form CH_2 and H_2O; path 2-8 is that via path 2-6 (CHOH intermediate) to form CH_2OH, followed by the C−O bond scission of CH_2OH with hydrogen assistance to form CH_2 and H_2O. Thus, we only describe the C−O bond scission of CH_2OH with hydrogen assistance to form CH_2 and H_2O via TS2-9; the activation barrier for this elementary reaction is 70.8 kJ·mol^{-1}, and the reaction is exothermic by 30.4 kJ·mol^{-1}.

On the basis of the above results, starting from CHO+H, we can obtain from Figure 6 that the highest barrier and reaction energy (27.0 and −86.4 kJ·mol^{-1}) of path 2-7 are lower than those of other pathways, which suggests that path 2-7 is more favorable both kinetically and thermodynamically than other pathways. Therefore, path 2-7 (CHO+H → CH_2O+H → CH_2OH+H → CH_2+H_2O) dominantly contributes to the formation of CH_2 from CHO hydrogenation on the Cu(110) surface. The rate-controlled step for path 2-7 occurs at TS2-6 with a corresponding activation barrier of 75.9 kJ·mol^{-1}.

3.1.6. CH_3 Formation. For CH_3 formation, five possible paths are considered, as shown in Figure 2, the potential energy diagram for these reaction pathways together with the structures of initial states, transition states, and final states are shown in Figure 7.

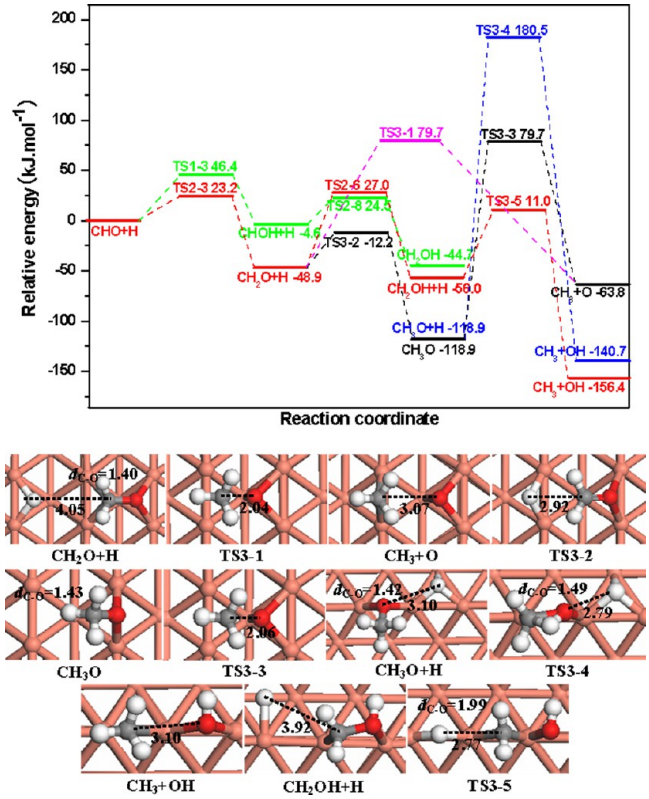

Figure 7. The potential energy profile for CH_3 formation together with the structures of initial states, transition states, and final states. Bond lengths are in Å. See Figure 3 for color coding.

For path 3-1, as described in path 2-3, CHO first hydrogenates to form CH_2O; then, the C−O bond scission of CH_2O with hydrogen assistance can form CH_3 and O via a transition state TS3-1. In the final state, CH_3+O, CH_3 adsorbs at the SB site, atomic O sits at a pseudo-fcc(111) site, and the distance between C and O atoms is 2.04 Å. The activation barrier and reaction energy for this elementary reaction are 128.6 and −14.9 kJ·mol^{-1}, respectively.

For path 3-2, as described in path 2-3, CHO first hydrogenates to form CH_2O; then, CH_2O can hydrogenate to form CH_3O via TS3-2. In TS3-2, CH_2O binds at the H site and the H adatom sits at a pseudo-fcc(111) site with the

dx.doi.org/10.1021/jp311701r | J. Phys. Chem. C 2013, 117, 6594−6606

distance between H adatom and C of 2.92 Å. The activation barrier of this elementary reaction is 36.7 kJ·mol^{-1}, and the reaction is found to be exothermic by 70.0 kJ·mol^{-1}. After that, the C−O bond scission of CH_3O can form CH_3 and O via TS3-3; in TS3-3, the distance between C and O atoms is elongated to 2.06 Å from 1.43 Å in CH_3O. This elementary reaction is endothermic by 55.1 kJ·mol^{-1} and with a high activation barrier of 198.6 kJ·mol^{-1}.

For path 3-3, as described in path 3-2, CHO first hydrogenates to form CH_3O; then, the C−O bond scission of CH_3O with hydrogen assistance can form CH_3 and OH via TS3-4; in TS3-4, CH_3O adsorbs at the SB site and a H adatom sits at a pseudo-fcc(111) site with the distance between H adatom and O of 2.79 Å. The activation barrier and reaction energy of this elementary reaction are 299.4 and −21.8 kJ·mol^{-1}, respectively.

For paths 3-4 and 3-5, as described in paths 2-5 and 2-6, CHO first hydrogenates via CH_2O and CHOH intermediates to form CH_2OH, respectively; then, the C−O bond scission of CH_2OH with hydrogen assistance leads to the formation of CH_3 and OH via TS3-5. In TS3-5, CH_2 locates at the SB site; OH binds above a Cu atom through an O atom, and atomic H sits at the SB site. This elementary reaction is exothermic by 100.4 kJ·mol^{-1} with an activation barrier of 67.0 kJ·mol^{-1}.

On the basis of the above results, starting from CHO+H, we can obtain from Figure 7 that the highest barrier and reaction energy (27.0 and −156.4 kJ·mol^{-1}) of path 3-4 are less than those of other pathways, which suggests that path 3-4 is more favorable both kinetically and thermodynamically than other pathways. Therefore, path 3-4 (CHO+H → CH_2O+H → CH_2OH+H → CH_3+OH) is mainly responsible for the formation of CH_3 from CHO hydrogenation on the Cu(110) surface. The rate-controlled step for path 3-4 occurs at TS2-6 with a corresponding activation barrier of 75.9 kJ·mol^{-1}.

3.1.7. Brief Summary. The above results show the initial step of CO hydrogenation to form CHO on the Cu(110) surface is more favorable both kinetically and thermodynamically than CO direct dissociation and COH formation. Then, all CH_x (x = 1−3) species are produced from CHO hydrogenation; Figure 8 presents the optimal paths for CH_x (x = 1−3) formation from CHO hydrogenation on the Cu(110) surface. Starting from CHO+H, the highest barriers for the formations of CH, CH_2, and CH_3 are 90.7, 27.0, and 27.0 kJ·mol^{-1} with the corresponding reaction energies of −45.6, −86.4, and −156.4 kJ·mol^{-1}, respectively. As a result, the formations of CH_2 and CH_3 are much easier than the formation of CH, and the formations of CH_2 and CH_3 have the same rate-controlled step occurring at TS2-6. Therefore, we can obtain that, among all CH_x (x = 1−3) species formed by CO hydrogenation, CH_2 and CH_3 are the most favored monomer on the Cu(110) surface.

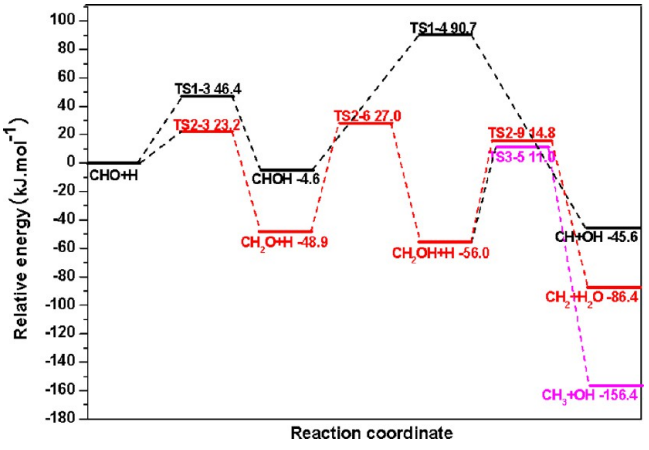

Figure 8. The potential energy profile for the optimal paths of CH_x (x = 1−3) formation starting from CHO hydrogenation on the Cu(110) surface.

3.2. CH_3OH Formation. As mentioned above, our results suggest that the initial step of CO hydrogenation can dominantly form CHO, and all CH_x (x = 1−3) species are formed by the dissociation of CH_xO and CH_xOH intermediates involved in CHO hydrogenation, in which CH_2 and CH_3 are the most favored monomer. Then, the C−C chain of C_2 oxygenates is formed by CO or CHO insertion into the CH_x (x = 2, 3) pathway. However, when above the reactions occur, the CH_xO and CH_xOH intermediates can also hydrogenate to form CH_3OH due to the general fact that Cu catalyst shows good catalytic performance for CH_3OH formation from syngas.[58] Thus, we further investigate the formation of CH_3OH by CHO hydrogenation. As shown in Figure 2, there are three possible pathways for CH_3OH formation, paths 4-1, 4-2, and 4-3. Figure 9 presents the corresponding potential energy diagram for these reaction pathways together with the initial states, transition states, and final states.

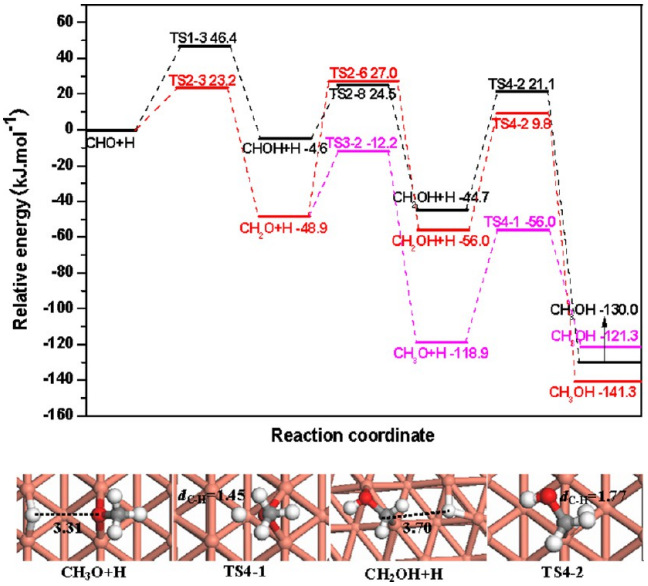

Figure 9. The potential energy profile for CH_3OH formation from CHO hydrogenation on the Cu(110) surface together with the structures of initial states, transition states, and final states. Bond lengths are in Å. See Figure 3 for color coding.

For path 4-1, as described in path 3-2, CHO first hydrogenates via a CH_2O intermediate to form CH_3O; then, CH_3O can hydrogenate to form CH_3OH via TS4-1. The activation barrier of this elementary reaction is 62.9 kJ·mol^{-1}, and the reaction is found to be slightly exothermic by 2.4 kJ·mol^{-1}. For path 4-2, as described in path 2-5, CHO first hydrogenates via CH_2O intermediate to form CH_2OH; then, CH_2OH hydrogenation leads to CH_3OH via TS4-2. In TS4-2, CH_2OH locates at the SB site, and the H adatom sits at a pseudo-fcc(111) site; the activation barrier and reaction energy of this elementary reaction are 65.8 and −85.3 kJ·mol^{-1}. For path 4-3, as described in path 2-6, CHO first hydrogenates via a

dx.doi.org/10.1021/jp311701r | J. Phys. Chem. C 2013, 117, 6594−6606

CHOH intermediate to form CH_2OH; then, CH_2OH hydrogenation leads to CH_3OH via TS4-2.

On the basis of the above results, we can see from Figure 9 that the highest barriers of paths 4-1 and 4-2 (23.2 and 27.0 kJ·mol^{-1}) are lower than that of path 4-3 (46.4 kJ·mol^{-1}). For paths 4-1 and 4-2, the rate-controlled step occurs at TS4-1 and TS2-6 and the corresponding activation barriers are 62.9 and 75.9 kJ·mol^{-1}. Therefore, path 4-1 (CHO+H → CH_2O+H → CH_3O+H → CH_3OH) is mainly responsible for the formation of CH_3OH from CHO hydrogenation on the Cu(110) surface.

3.3. Comparisons between CH_3OH and CH_x (x = 2, 3) Formations. Figure 10 presents the potential energy diagram

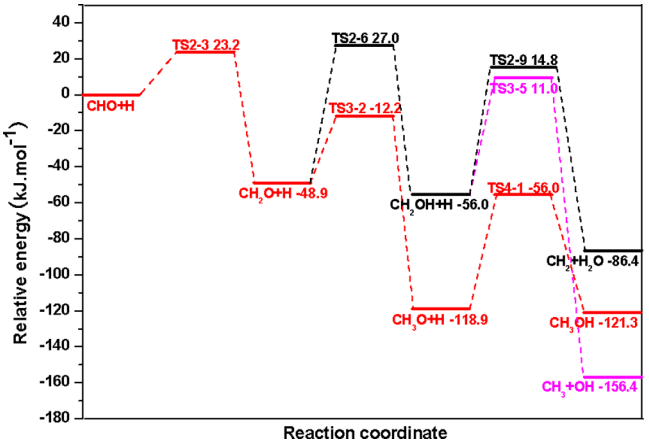

Figure 10. The potential energy profile for the optimal paths of CH_x (x = 2, 3) and CH_3OH formation starting from CHO hydrogenation on the Cu(110) surface.

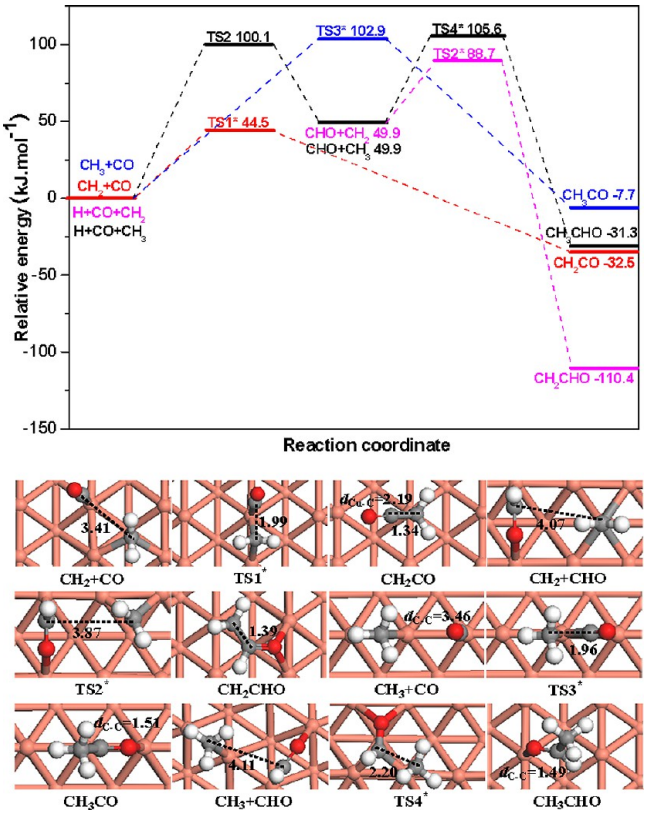

Figure 11. The potential energy profile for CO and CHO insertion into CH_x (x = 2, 3) on the Cu(110) surface together with the structures of initial states, transition states, and final states. Bond lengths are in Å. See Figure 3 for color coding.

for the optimal paths of CH_x (x = 2−3) and CH_3OH formation starting from CHO hydrogenation on the Cu(110) surface; we can see that the formation of CH_2, CH_3, and CH_3OH has approximate highest barriers of 27.0, 27.0, and 23.2 kJ·mol^{-1} with the reaction energies of −86.4, −156.4, and −121.3 kJ·mol^{-1}. However, for the formation of CH_2, CH_3, and CH_3OH, the rate-controlled step occurs at TS2-6, TS2-6, and TS4-1 and the corresponding activation barriers are 75.9, 75.9, and 62.9 kJ·mol^{-1}. Therefore, CH_3OH is the preferable product by CO hydrogenation on the Cu(110) surface and the formation of CH_2 and CH_3 cannot compete with the formation of CH_3OH.

3.4. C−C Chain Formation of C_2 Oxygenates. As mentioned above, among all CH_x (x = 1−3) species, CH_2 and CH_3 are the most favored monomers by CO hydrogenation on the Cu(110) surface. Moreover, previous studies by Zhao et al.[14] have shown that CHO insertion into CH_x (x = 1−3) is superior and/or competitive to CO insertion into CH_x for the C−C chain formation of C_2 oxygenates on Rh(111) and Co(0001) surfaces; as a result, in this study, we consider the C−C chain formation of C_2 oxygenates proceed by CO or CHO insertion into CH_x (x = 2, 3) on the Cu(110) surface. The potential energy diagram for these reactions together with the structures of initial states, transition states, and final states are illustrated in Figure 11.

3.4.1. CO or CHO Insertion into CH_2. For CO insertion into CH_2, starting from CH_2+CO, CH_2 binds through its C atom at the H site, and CO sits at the T site, CH_2 can interact with CO to form CH_2CO via a transition state TS1*; in TS1*, CH_2 locates at the SB site; CO sits at the T site, and CH_2 and CO share one Cu atom with a shortened C−C distance of 1.99 Å. The activation barrier of this elementary reaction is 44.5 kJ·mol^{-1}, and the reaction is exothermic by 32.5 kJ·mol^{-1}. CH_2CO adsorbs at the T site through the C atom of CH_2 with a C−Cu bond length of 2.19 Å, which has an adsorption energy of 54.6 kJ·mol^{-1}.

For CHO insertion into CH_2, in the initial state, CH_2+CHO, CH_2 binds through its C atom at the H site, and CHO adsorbs at the LB site through both C and O atoms, the interaction between CH_2 and CHO can form CH_2CHO via TS2*, in TS2*, CH_2 adsorbs at the pseudo-fcc(111) site, and CHO binds at the LB site with a shortened C−C distance of 3.87 Å. This elementary reaction has an activation barrier of 38.8 kJ·mol^{-1}, and the reaction is largely exothermic by 160.3 kJ·mol^{-1}. CH_2CHO locates at the H site via both C and O atoms, and the corresponding adsorption energy is 269.4 kJ·mol^{-1}.

3.4.2. CO or CHO Insertion into CH_3. For CO insertion into CH_3, starting from CH_3+CO, CH_3 binds at the SB site through a C atom, CO sits at the T site through a C atom, and CH_3 reacts with CO to form CH_3CO via TS3*; in TS3*, CH_3 binds at the SB site; CO sits at the T site sharing one Cu atom with CH_3 with a shortened C−C distance of 1.96 Å. The activation barrier of this elementary reaction is 102.9 kJ·mol^{-1}, and the reaction is found to be slightly exothermic by 7.7 kJ·mol^{-1}. CH_3CO locates at the SB site through both C and O atoms, which has an adsorption energy of 212.1 kJ·mol^{-1}.

For CHO insertion into CH_3, beginning with CH_3+CHO, CH_3 binds through a C atom at the SB site, CHO adsorbs at the LB site through both C and O atoms, and CH_3 can interact

dx.doi.org/10.1021/jp311701r | J. Phys. Chem. C 2013, 117, 6594−6606

with CHO to form CH_3CHO via TS4*; in TS4*, CHO binds at the H site, CH_3 adsorbs at the T site sharing one Cu atom with CH_3, and the C−C distance is 2.20 Å. This elementary reaction has an activation barrier of 55.7 kJ·mol^{-1}, and the reaction is exothermic by 81.2 kJ·mol^{-1}. CH_3CHO locates at the T site through an O atom with an adsorption energy of 56.0 kJ·mol^{-1}.

3.4.3. Brief Summary. On the basis of the above results, for the reactions of CH_2 or CH_3 insertion into CHO, considering the reaction energy of CHO formation by CO hydrogenation, we can see from Figure 11 that the highest barriers for CO insertion into CH_2 (44.5 kJ·mol^{-1}) are smaller than those for CO insertion into CH_3 (102.9 kJ·mol^{-1}), CHO insertion into CH_2 (105.6 kJ·mol^{-1}), and CHO insertion into CH_3 (100.1 kJ·mol^{-1}). As a result, the C−C chain formation of C_2 oxygenates by CO insertion into CH_2 is more favorable kinetically than those by CHO insertion into CH_x (x = 2, 3) and CO insertion into CH_3.

3.5. Comparisons between CO Insertion into CH_x (x = 2, 3) and the Hydrogenation, Dissociation, and Coupling of CH_x (x = 2, 3). Previous studies by Choi and Liu[7] have shown that the productivity and selectivity for C_2 oxygenates are controlled by CH_4 formation on the Rh(111) surface; further, Zhao et al.[14] have suggested that the C−C chain formation by CHO or CO insertion into CH_x and carbene coupling is competitive on Rh and Co surfaces. Therefore, on the Cu(110) surface, we further discuss the coupling of CH_x (x = 2, 3) to form C_2H_4 and C_2H_6, CH_x (x = 2, 3) hydrogenation to form CH_3 and CH_4, as well as CH_x (x = 2, 3) dissociation to form CH and CH_2, respectively. Figure 11 presents the potential energy diagram for these reactions together with the structures of initial states, transition states, and final states.

3.5.1. The Hydrogenation, Dissociation, and Coupling of CH_2. For CH_2 hydrogenation, starting from CH_2+H, CH_2 adsorbs at the hollow site and H binds at the pseudo-fcc(111) site; both are the most stable configurations for CH_2 and H species on the Cu(110) surface. The H adatom moves toward the C atom of adsorbed CH_2 via a transition state TS1′ to form CH_3; in TS1′, the distance between C and H atoms is shortened to 1.81 Å from 3.08 Å in CH_2+H; this elementary reaction is exothermic by 95.2 kJ·mol^{-1} with an activation barrier of 61.1 kJ·mol^{-1}.

For CH_2 dissociation, beginning from CH_2, the C−H bond cleavage of CH_2 can form CH and H via TS2′. In TS2′, CH binds at the hollow site through a C atom and H adsorbs at the LB site with a substantially elongated C−H bond of 1.81 Å. In the final state, CH+H, CH sits at the hollow site and H binds at the pseudo-fcc(111) site. The activation barrier for this elementary reaction is 103.1 kJ·mol^{-1}, and the reaction is endothermic by 50.1 kJ·mol^{-1}.

For CH_2 coupling, in the initial state, CH_2+CH_2, two CH_2 bind through a C atom at two adjacent hollow sites; the interaction between CH_2 and CH_2 can form C_2H_4 via TS3′. In TS3′, the distance of two C atoms is shortened to 3.27 Å from 3.59 Å in the initial state. This elementary reaction has an activation barrier of 82.1 kJ·mol^{-1}, and the reaction is largely exothermic by 158.4 kJ·mol^{-1}.

On the basis of the above results, we can see from Figure 12a that the coupling of CH_2 to form the C−C chain of C_2H_4 is unfavorable in dynamics in comparison with CO insertion into CH_2 for C−C chain formation of C_2 oxygenates; meanwhile, CH_2 hydrogenation and dissociation cannot compete with the

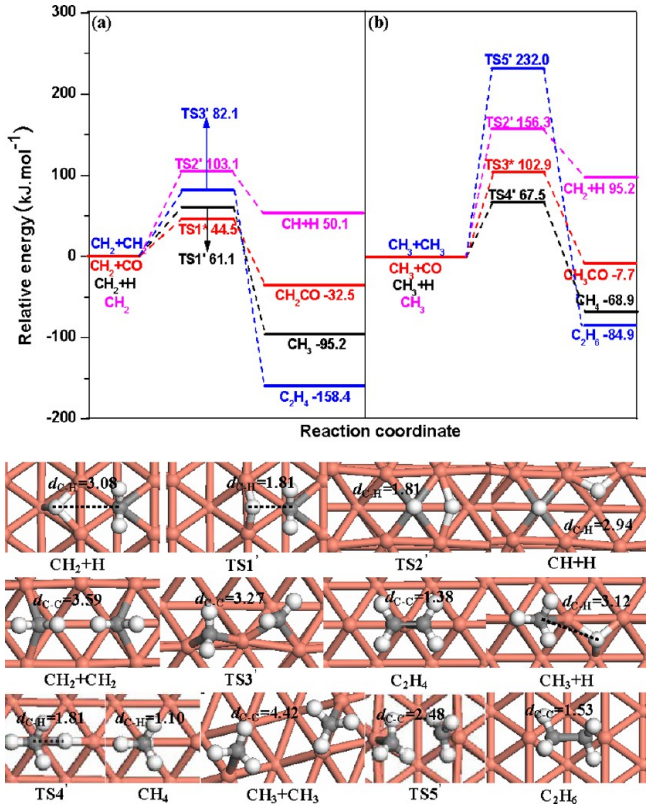

Figure 12. The activation barriers and reaction energies for the hydrogenation, dissociation, and coupling of CH_x (x = 2, 3) as well as CO insertion into CH_x (x = 2, 3) on the Cu(110) surface together with the structures of initial states, transition states, and final states. Bond lengths are in Å. See Figure 3 for color coding.

C−C chain formation of C_2 oxygenates by CO insertion into CH_2; namely, CO insertion into CH_2 is the dominant reaction for CH_2 on the Cu(110) surface.

3.5.2. The Hydrogenation, Dissociation, and Coupling of CH_3. For CH_3 hydrogenation, starting from CH_3+H, CH_3 adsorbs at the SB site and H binds at the pseudo-fcc(111) site; both are the most stable configurations for CH_3 and H species on the Cu(110) surface. The H adatom moves toward the C atom of adsorbed CH_3 via TS4′ to form CH_4; in TS4′, the distance between C and H atoms is shortened to 1.81 Å from 3.12 Å in CH_3+H; this elementary reaction is exothermic by 68.9 kJ·mol^{-1} with an activation barrier of 67.5 kJ·mol^{-1}.

For CH_3 dissociation, it is the reverse reaction of CH_2 hydrogenation, this elementary reaction is endothermic by 95.2 kJ·mol^{-1} with a high activation barrier of 156.3 kJ·mol^{-1}.

For CH_3 coupling, in the initial state, CH_3+CH_3, two CH_3 bind through a C atom at two adjacent SB sites and CH_3 coupling can form C_2H_6 via TS5′. In TS5′, the distance between C and C is shortened to 2.48 Å from 4.42 Å in the initial state. This elementary reaction has a significant activation barrier of 232.0 kJ·mol^{-1}, and the reaction is largely exothermic by 84.9 kJ·mol^{-1}.

On the basis of the above results, we can see from Figure 12b that CH_3 coupling to form the C−C chain of C_2H_6 is unfavorable in dynamics in comparison with CH_3 hydrogenation; meanwhile, CH_3 dissociation and CO or CHO insertion into CH_3 cannot compete with CH_3 hydrogenation to form CH_4; namely, CH_3 hydrogenation to form CH_4 is the dominant reaction for the CH_3 on the Cu(110) surface.

dx.doi.org/10.1021/jp311701r | J. Phys. Chem. C 2013, 117, 6594−6606

3.6. General Discussion. Overall, our DFT calculations show that CH_3OH is the most favorable product for CO hydrogenation rather than CH_x (x = 1−3) species on the Cu(110) surface, which agrees well with the general fact that Cu catalysts show good catalytic performance for CH_3OH formation from syngas.[58] Then, among all CH_x (x = 1−3) species formed by CO hydrogenation, CH_2 and CH_3 are the most favored monomers on the Cu(110) surface. Further, for CH_2, CO insertion into CH_2 to form C_2 oxygenates is the dominant reaction among all reactions related to CH_2 on the Cu(110) surface with an activation barrier of 44.5 kJ·mol^{-1}; for CH_3, CH_3 hydrogenation to form CH_4 is the dominant reaction with an activation barrier of 67.5 kJ·mol^{-1} on the Cu(110) surface. As a result, C_2 oxygenates can be formed from syngas only by CO insertion into CH_2 on the Cu(110) surface; namely, CH_2 is the most favored CH_x monomer, leading to C−C chain formation of C_2 oxygenates. Finally, on the basis of the above results, Cu(110) is highly selective for the formation of CH_3OH from syngas rather than the formation of C_2 oxygenates and CH_4.

On the other hand, according to our analysis, two variables significantly determine the productivity and selectivity of C_2 oxygenates from syngas; one is the barrier of CH_3OH formation, and the other is the barrier of CH_2 or CH_3 formation. By lowering the barrier of CH_2 formation and/or suppressing CH_3OH and CH_3 production, in this way, CH_3OH and CH_3 formation cannot compete with CH_2 resources. More CH_2 will be available for the C−C chain formation of C_2 oxygenates; as a result, the productivity and selectivity of C_2 oxygenates can be improved. Our results mean that, to achieve the high productivity and selectivity of C_2 oxygenates, promoters and/or supports to the Cu are necessary, which should help facilitate CH_2 formation and/or minimize CH_3OH and CH_3 production.

Therefore, when Cu-based catalysts are employed for C_2 oxygenate formation from syngas, the catalytic activities of the materials toward CH_2, CH_3, and CH_3OH formation have to be especially considered. To achieve high productivity and selectivity of C_2 oxygenates, the promoters and/or supports used for Cu catalysts should maximize CH_2 and/or minimize CH_3OH and CH_3 formation. More importantly, our results suggest that the fundamental insight into the reaction mechanism of CH_x (x = 1−3) and C−C chain formation from syngas on Cu catalyst not only provide the significant understanding of how the Cu catalyst functions in the formation of C_2 oxygenates but also provide a clue for the selective modification and development of novel Cu-based catalyst to improve catalytic performance toward the desired products. In addition, quantitative investigations into the effect of the promoters and/or supports on C_2 oxygenate formation with extensive calculations would be desirable, but this is beyond the scope of the present study.

4. CONCLUSIONS

In this study, the density functional theory method together with the periodic slab model have been employed to systematically investigate the preference formation mechanism of CH_x (x = 1−3) and C−C chain involved in C_2 oxygenate formation from syngas on the Cu(110) surface. Our results show that CO direct dissociation is not energetically favored on the Cu(110) surface, and CO hydrogenation to form CHO is more favorable both kinetically and thermodynamically than COH formation. Then, starting from CHO, CH_x (x = 1−3) formation under two conditions, without or with hydrogen assistance, is considered to obtain the optimal paths, suggesting that, among all CH_x (x = 1−3) species, CH_2 and CH_3 are the most favored monomers. Further, CH_3OH is the preferable product from syngas on the Cu(110) surface, and the formation of CH_x cannot compete with the formation of CH_3OH.

On the basis of the most favored monomer, CH_2 and CH_3, we further probe into the C−C chain formation by CO and CHO insertion into CH_x (x = 2, 3), and CH_x (x = 2, 3) hydrogenation and dissociation, as well as the coupling of CH_x (x = 2, 3) to form C_2H_4 and C_2H_6. Our results show that CO insertion into CH_2 to form C_2 oxygenates is the dominant reaction among all reactions related to CH_2 on the Cu(110) surface. For CH_3, CH_3 hydrogenation to form CH_4 is the dominant reaction on the Cu(110) surface. Meanwhile, our results show that CO insertion into CH_2 is dominantly responsible for C_2 oxygenate formation from syngas on the Cu(110) surface. Finally, to achieve high productivity and selectivity of C_2 oxygenates, the promoters and/or supports used for Cu catalysts are necessary, which should help facilitate CH_2 formation and/or minimize CH_3OH and CH_3 production.

AUTHOR INFORMATION

Corresponding Author

*Address: No. 79 Yingze West Street, Taiyuan 030024, China. Phone: +86 351 6018239. Fax: +86 351 6041237. E-mail: wangbaojun@tyut.edu.cn, quantumtyut@126.com.

Notes

The authors declare no competing financial interest.

ACKNOWLEDGMENTS

This work is supported by the National Natural Science Foundation of China (21276003, 20906066, and 21276171). The authors especially thank two anonymous reviewers for their helpful suggestions on the quality improvement of our present paper.

REFERENCES

(1) Goldemberg, J. Ethanol for a Sustainable Energy Future. *Science* **2007**, *315*, 808−810.

(2) Gong, J.; Yue, H.; Zhao, Y.; Zhao, S.; Zhao, L.; Lv, J.; Wang, S.; Ma, X. Synthesis of Ethanol via Syngas on Cu/SiO_2 Catalysts with Balanced Cu^0-Cu^+ Sites. *J. Am. Chem. Soc.* **2012**, *134*, 13922−13925.

(3) Gupta, M.; Smith, M. L.; Spivey, J. Heterogeneous Catalytic Conversion of Dry Syngas to Ethanol and Higher Alcohols on Cu-Based Catalysts. *ACS Catal.* **2011**, *1*, 641−656.

(4) Spivey, J. J.; Egbebi, A. Heterogeneous Catalytic Synthesis of Ethanol from Biomass-Derived Syngas. *Chem. Soc. Rev.* **2007**, *36*, 1514−1528.

(5) Subramani, V.; Gangwal, S. K. Review of Recent Literature to Search for an Efficient Catalytic Process for the Conversion of Syngas to Ethanol. *Energy Fuels* **2008**, *22*, 814−839.

(6) Herman, R. G. Advances in Catalytic Synthesis and Utilization of Higher Alcohols. *Catal. Today* **2000**, *55*, 233−245.

(7) Choi, Y.; Liu, P. Mechanism of Ethanol Synthesis from Syngas on Rh(111). *J. Am. Chem. Soc.* **2009**, *131*, 13054−13061.

(8) Han, L.; Mao, D.; Yu, J.; Guo, Q.; Lu, G. Synthesis of C_2-Oxygenates from Syngas over Rh-Based Catalyst Supported on SiO_2, TiO_2 and SiO_2-TiO_2 Mixed Oxide. *Catal. Commun.* **2012**, *23*, 20−24.

(9) Zhao, Y. H.; Yang, M. M.; Sun, D.; Su, H. Y.; Sun, K.; Ma, X.; Bao, X.; Li, W. X. Rh-Decorated Cu Alloy Catalyst for Improved C_2 Oxygenate Formation from Syngas. *J. Phys. Chem. C* **2011**, *115*, 18247−18256.

(10) Kapur, N.; Hyun, J.; Shan, B.; Nicholas, J. B.; Cho, K. Ab Initio Study of CO Hydrogenation to Oxygenates on Reduced Rh Terraces and Stepped Surfaces. *J. Phys. Chem. C* **2010**, *114*, 10171−10182.
(11) Subramanian, N. D.; Balaji, G.; Kumar, C. S. S. R.; Spivey, J. J. Development of Cobalt−Copper Nanoparticles as Catalysts for Higher Alcohol Synthesis from Syngas. *Catal. Today* **2009**, *147*, 100−106.
(12) Haider, M. A.; Gogate, M. R.; Davis, R. J. Fe-Promotion of Supported Rh Catalysts for Direct Conversion of Syngas to Ethanol. *J. Catal.* **2009**, *261*, 9−16.
(13) Gronchi, P.; Tempesti, E.; Mazzocchia, C. Metal Dispersion Dependent Selectivities for Syngas Conversion to Ethanol on V_2O_3 Supported Rhodium. *Appl. Catal., A* **1994**, *120*, 115−126.
(14) Zhao, Y. H.; Sun, K.; Ma, X.; Liu, J.; Sun, D.; Su, H. Y.; Li, W. X. Carbon Chain Growth by Formyl Insertion on Rhodium and Cobalt Catalysts in Syngas Conversion. *Angew. Chem., Int. Ed.* **2011**, *50*, 5335−5338.
(15) Slaa, J. C.; van Ommen, J. G.; Ross, J. R. H. The Synthesis of Higher Alcohols Using Modified $Cu/ZnO/Al_2O_3$ Catalysts. *Catal. Today* **1992**, *15*, 129−148.
(16) Xu, R.; Wei, W.; Li, W. H.; Hu, T. D.; Sun, Y. H. Fe Modified $CuMnZrO_2$ Catalysts for Higher Alcohols Synthesis from Syngas: Effect of Calcination Temperature. *J. Mol. Catal. A: Chem.* **2005**, *234*, 75−83.
(17) Xu, R.; Yang, C.; Wei, W.; Li, W.; Sun, Y.; Hu, T. Fe-modified $CuMnZrO_2$ Catalysts for Higher Alcohols Synthesis from Syngas. *J. Mol. Catal. A: Chem.* **2004**, *221*, 51−58.
(18) Zhao, N.; Xu, R.; Wei, W.; Sun, Y. $Cu/Mn/ZrO_2$ Catalyst for Alcohol Synthesis by Fischer−Tropsch Modified Elements. *React. Kinet. Catal. Lett.* **2002**, *75*, 297−304.
(19) Mahdavi, V.; Peyrovi, M. H.; Islami, M.; Mehr, J. Y. Synthesis of Higher Alcohols from Syngas over $Cu\text{-}Co_2O_3/ZnO$, Al_2O_3 Catalyst. *Appl. Catal., A* **2005**, *281*, 259−265.
(20) Cheng, J.; Hu, P.; Ellis, P.; French, S.; Kelly, G.; Lok, C. M. A First-Principles Study of Oxygenates on Co Surfaces in Fischer−Tropsch Synthesis. *J. Phys. Chem. C* **2008**, *112*, 9464−9473.
(21) Zhang, R. G.; Wang, B. J.; Liu, H. Y.; Ling, L. X. Effect of Surface Hydroxyls on CO_2 Hydrogenation over $Cu/\gamma\text{-}Al_2O_3$ Catalyst: A Theoretical Study. *J. Phys. Chem. C* **2011**, *115*, 19811−19818.
(22) Mei, D. H.; Neurock, M.; Smith, C. M. Hydrogenation of Acetylene-Ethylene Mixtures over Pd and Pd-Ag Alloys: First-Principles-Based Kinetic Monte Carlo Simulations. *J. Catal.* **2009**, *268*, 181−195.
(23) Chin, Y. H.; Buda, C.; Neurock, M.; Iglesia, E. Selectivity of Chemisorbed Oxygen in C−H Bond Activation and CO Oxidation and Kinetic Consequences for $CH_4\text{-}O_2$ Catalysis on Pt and Rh Clusters. *J. Catal.* **2011**, *283*, 10−24.
(24) Huo, C. F.; Li, Y. W.; Wang, J. G.; Jiao, H. J. Insight into CH_4 Formation in Iron-Catalyzed Fischer−Tropsch Synthesis. *J. Am. Chem. Soc.* **2009**, *131*, 14713−14721.
(25) Liu, Z. P.; Hu, P. General Rules for Predicting Where a Catalytic Reaction Should Occur on Metal Surfaces: A Density Functional Theory Study of C−H and C−O Bond Breaking/Making on Flat, Stepped, and Kinked Metal Surfaces. *J. Am. Chem. Soc.* **2003**, *125*, 1958−1967.
(26) Pan, Y. X.; Liu, C. J.; Ge, Q. F. Adsorption and Protonation of CO_2 on Partially Hydroxylated $\gamma\text{-}Al_2O_3$ Surfaces: A Density Functional Theory Study. *Langmuir* **2008**, *24*, 12410−12419.
(27) Pan, Y. X.; Liu, C. J.; Ge, Q. F. Effect of Surface Hydroxyls on Selective CO_2 Hydrogenation over $Ni_4/\gamma\text{-}Al_2O_3$: A Density Functional Theory Study. *J. Catal.* **2010**, *272*, 227−234.
(28) Zhang, R. G.; Liu, H. Y.; Wang, B. J.; Ling, L. X. Insights into the Effect of Surface Hydroxyls on CO_2 Hydrogenation over $Pd/\gamma\text{-}Al_2O_3$ Catalyst: A Computational Study. *Appl. Catal., B* **2012**, *126*, 108−120.
(29) Bowker, M.; Madix, R. J. XPS, UPS and Thermal Desorption Studies of Alcohol Adsorption on Cu(110). *Surf. Sci.* **1980**, *95*, 190−206.
(30) Russell, J. N.; Gates, S. M.; Yates, J. T. Reaction of Methanol with Cu(111) and Cu(111)+O(ads). *Surf. Sci.* **1985**, *163*, 516−540.
(31) Sexton, B. A. Surface Vibrations of Adsorbed Intermediates in the Reaction of Alcohols with Cu(100). *Surf. Sci.* **1979**, *88*, 299−318.
(32) Nakamura, J.; Canpbell, J. M.; Campbell, C. T. Kinetics and Mechanism of the Water-Gas Shift Reaction Catalysed by the Clean and Cs-Promoted Cu(110) Surface: A Comparison with Cu(111). *J. Chem. Soc., Faraday Trans.* **1990**, *86*, 2725−2734.
(33) Lee, J.; Sorescu, D. C.; Jordan, K. D.; Yates, J. T. Hydroxyl Chain Formation on the Cu(110) Surface: Watching Water Dissociation. *J. Phys. Chem. C* **2008**, *112*, 17672−17677.
(34) Jakdetchai, O.; Nakajima, T. Mechanism of the Water-Gas Shift Reaction over Cu(110), Cu(111) and Cu(100) Surfaces: An AM1-D Study. *J. Mol. Struct.: THEOCHEM* **2002**, *619*, 51−58.
(35) Ren, J.; Meng, S. Atomic Structure and Bonding of Water Overlayer on Cu(110): The Borderline for Intact and Dissociative Adsorption. *J. Am. Chem. Soc.* **2006**, *128*, 9282−9283.
(36) Grabow, L. C.; Mavrikakis, M. Mechanism of Methanol Synthesis on Cu through CO_2 and CO Hydrogenation. *ACS Catal.* **2011**, *1*, 365−384.
(37) Kresse, G.; Joubert, D. From Ultrasoft Pseudopotentials to the Projector Augmented-Wave Method. *Phys. Rev. B* **1999**, *59*, 1758−1775.
(38) Kresse, G.; Hafner, J. Ab Initio Molecular Dynamics for Liquid Metals. *Phys. Rev. B* **1993**, *47*, 558−561.
(39) Kresse, G.; Furthmuller, J. Efficient Iterative Schemes for Ab Initio Total-Energy Calculations Using a Plane-Wave Basis Set. *Phys. Rev. B* **1996**, *54*, 11169−11186.
(40) Kresse, G.; Furthmuller, J. Efficiency of Ab-initio Total Energy Calculations for Metals and Semiconductors Using a Plane-Wave Basis Set. *Comput. Mater. Sci.* **1996**, *6*, 15−50.
(41) Perdew, J. P.; Chevary, J. A.; Vosko, S. H.; Jackson, K. A.; Pederson, M. R.; Singh, D. J.; Fiolhais, C. Atoms, Molecules, Solids, and Surfaces: Applications of the Generalized Gradient Approximation for Exchange and Correlation. *Phys. Rev. B* **1992**, *46*, 6671−6687.
(42) Monkhorst, H. J.; Pack, J. D. Special Points for Brillouin-Zone Integrations. *Phys. Rev. B* **1976**, *13*, 5188−5192.
(43) Methfessel, M.; Paxton, A. T. High-Precision Sampling for Brillouin-Zone Integration in Metals. *Phys. Rev. B* **1989**, *40*, 3616−3621.
(44) Sheppard, D.; Xiao, P.; Chemelewski, W.; Johnson, D. D.; Henkelman, G. A Generalized Solid-State Nudged Elastic Band Method. *J. Chem. Phys.* **2012**, *136*, 074103-1−074103-08.
(45) Sheppard, D.; Terrell, R.; Henkelman, G. Optimization Methods for Finding Minimum Energy Paths. *J. Chem. Phys.* **2008**, *128*, 134106-1−134106-10.
(46) Henkelman, G.; Jónsson, H. A Dimer Method for Finding Saddle Points on High Dimensional Potential Surfaces Using Only First Derivatives. *J. Chem. Phys.* **1999**, *111*, 7010−7022.
(47) Olsen, R. A.; Kroes, G. J.; Henkelman, G.; Arnaldsson, A.; Jónsson, H. Comparison of Methods for Finding Saddle Points without Knowledge of the Final States. *J. Chem. Phys.* **2004**, *121*, 9776−9792.
(48) Zhang, R. G.; Ling, L. X.; Wang, B. J.; Huang, W. Solvent Effects on Adsorption of CO over CuCl(111) Surface: A Density Functional Theory Study. *Appl. Surf. Sci.* **2010**, *256*, 6717−6722.
(49) Sun, B. Z.; Chen, W. K.; Zheng, J. D.; Lu, C. H. Roles of Oxygen Vacancy in the Adsorption Properties of CO and NO on $Cu_2O(111)$ Surface: Results of a First-Principles Study. *Appl. Surf. Sci.* **2008**, *255*, 3141−3148.
(50) Jardillier, N.; Villagomez, E. A.; Delahay, G.; Coq, B.; Berthomieu, D. Probing Cu^{I}-Exchanged Zeolite with CO: DFT Modeling and Experiment. *J. Phys. Chem. B* **2006**, *110*, 16413−16421.
(51) Weilach, C.; Kozlov, S. M.; Holzapfel, H. H.; Fottinger, K.; Neyman, K. M.; Rupprechter, G. Geometric Arrangement of Components in Bimetallic PdZn/Pd(111) Surfaces Modified by CO Adsorption: A Combined Study by Density Functional Calculations, Polarization-Modulated Infrared Reflection Absorption Spectroscopy,

and Temperature-Programmed Desorption. *J. Phys. Chem. C* **2012**, *116*, 18768−18778.
(52) Loffreda, D.; Sautet, P. First-Principles Study of CO Adsorption and Vibration on Au Surfaces. *J. Phys. Chem. B* **2005**, *109*, 9596−9603.
(53) Flemmig, B.; Kretzschmar, I.; Friend, C. M.; Hoffmann, R. The Cyclopropylmethyl-3-Butenyl Rearrangement on Mo(110): A Radical Clock on a Surface? *J. Phys. Chem. A* **2004**, *108*, 2972−2981.
(54) Classen, T.; Lingenfelder, M.; Wang, Y.; Chopra, R.; Virojanadara, C.; Starke, U.; Costantini, G. Hydrogen and Coordination Bonding Supramolecular Structures of Trimesic Acid on Cu(110). *J. Phys. Chem. A* **2007**, *111*, 12589−12603.
(55) Pang, X.; Wang, C.; Zhou, Y.; Zhao, J.; Wang, G. DFT Study of the Structure Sensitivity for the Adsorption of Methyl, Methoxy, and Formate on Ni(111), Ni(100), and Ni(110) Surfaces. *J. Mol. Struct.: THEOCHEM* **2010**, *948*, 1−10.
(56) Szukiewicz, R.; Kołaczkiewicz, J.; Yakovkin, I. N. Zigzag Chain Structures of Gd on the Mo(110) Surface. *Surf. Sci.* **2008**, *602*, 2610−2616.
(57) Liao, D.; Glassford, K. M.; Ramprasad, R.; Adams, J. B. DFT-LDA Study of NO Adsorption on Rh(110) Surface. *Surf. Sci.* **1998**, *415*, 11−19.
(58) Behrens, M.; Studt, F.; Kasatkin, I.; Kühl, S.; Hävecker, M.; Abild-Pedersen, F.; Zander, S.; Girgsdies, F.; Kurr, P.; Kniep, B. L.; Tovar, M.; Fischer, R. W.; Nørskov, J. K.; Schlögl, R. The Active Site of Methanol Synthesis over $Cu/ZnO/Al_2O_3$ Industrial Catalysts. *Science* **2012**, *336*, 893−897.
(59) Remediakis, I. N.; Abild-Pedersen, F.; Nørskov, J. K. DFT Study of Formaldehyde and Methanol Synthesis from CO and H_2 on Ni(111). *J. Phys. Chem. B* **2004**, *108*, 14535−14540.
(60) Ojeda, M.; Li, A.; Nabar, R.; Nilekar, A. U.; Mavrikakis, M.; Iglesia, E. Kinetically Relevant Steps and H_2/D_2 Isotope Effects in Fischer−Tropsch Synthesis on Fe and Co Catalysts. *J. Phys. Chem. C* **2010**, *114*, 19761−19770.
(61) Zhang, Q.; Han, B.; Tang, X.; Heier, K.; Li, J. X.; Hoffman, J.; Lin, M.; Britton, S. L.; Derecskei-Kovacs, A.; Cheng, H. On the Mechanisms of Carbon Formation Reaction on Ni(111) Surface. *J. Phys. Chem. C* **2012**, *116*, 16522−16531.
(62) Li, H.; Chang, C.; Ho, J. Density Functional Calculations to Study the Mechanism of the Fischer−Tropsch Reaction on Fe(111) and W(111) Surfaces. *J. Phys. Chem. C* **2011**, *115*, 11045−11055.
(63) Mei, D.; Xu, L.; Henkelman, G. Potential Energy Surface of Methanol Decomposition on Cu(110). *J. Phys. Chem. C* **2009**, *113*, 4522−4537.
(64) Sexton, B. A.; Hughes, A. E.; Avery, N. R. A Spectroscopic Study of the Adsorption and Reactions of Methanol, Formaldehyde and Methyl Formate on Clean and Oxygenated Cu(110) Surfaces. *Surf. Sci.* **1985**, *155*, 366−386.
(65) Wachs, I. E.; Madix, R. J. The Selective Oxidation of CH_3OH to H_2CO on a Copper(110) Catalyst. *J. Catal.* **1978**, *53*, 208−227.